Effect of Disturbance of Inlet Spray Velocity on Flame Structure

T. Kitano, R. Kurose*, S. Komori
Department of Mechanical Engineering and Science, and Advanced Research Institute of Fluid Science and Engineering, Kyoto University, Yoshida-honmachi, Sakyo-ku, Kyoto, Kyoto 606-8501, Japan
kitano.tomoaki.88x@st.kyoto-u.ac.jp, kurose@mech.kyoto-u.ac.jp, and komori@mech.kyoto-u.ac.jp

Abstract

Effects of disturbances of inlet flow and spray velocities and internal pressure on spray combustion field are investigated by means of two-dimensional direct numerical simulation (DNS). n-decane ($C_{10}H_{22}$) is used as liquid spray fuel, and the evaporating droplets' motions are tracked by a Lagrangian manner. The pressure disturbance is captured by employing a pressure-based semi-implicit algorithm for compressible flows. The frequency and magnitude of the inlet disturbance are set at 800 Hz and up to 50 %, respectively, and the internal pressure is set at 0.1 or 0.5 MPa. The results show that the pressure perturbation in the spray combustion filed is enhanced by combustion reaction and increase in internal pressure, but it is not affected by inlet disturbances very much. The frequency indicating the frequency indicating the peak of power spectra of pressure perturbation depends on neither the inlet disturbance nor the internal pressure.

Introduction

From the viewpoint of environmental protection and energy security, it is extremely important to reduce CO_2 emitted by the consumption of fossil fuels in internal combustion engines such as gas turbine engine and diesel engine for energy conversion and propulsion devises. In order to optimally design and operate such equipments, precise prediction of the combustion behavior is essential. However, since combustion is a complex phenomenon, the prediction of the combusting flow behavior has been based on the engineers' experiences and the reliable prediction technique has not been well developed yet. In particular, spray combustion is a complex phenomenon in which liquid fuel is used and the dispersion of the liquid fuel droplets, their evaporation, and the chemical reaction of the fuel vapor with the oxidizer take place interactively at the same time. Hence, the underlying physics governing these processes has not been well understood [1],[2],[3],[4]. One of the most important issues of combustion research is the prediction and suppression of combustion instabilities. In spite of a large number of studies, however, the mechanism of the combustion instabilities has not been well clarified yet e.g.[5]. In particular, the mechanism of combustion instabilities for spray combustion is hardly understood. Recently, de la Cruz Garci'a et al. [6] investigated the self-excited oscillation in a kerosene spray flame by experiment and found that frequency of the self-excited oscillation depends on the degree of mixing of air and fuel droplets. However, the trigger of the self-excited oscillation is not clear.

In this study, effects of disturbances of inlet flow and spray velocities and internal pressure on spray combustion field are investigated by means of two-dimensional direct numerical simulation (DNS). n-decane ($C_{10}H_{22}$) is used as liquid spray fuel, and evaporating droplets' motions are tracked by a Lagrangian manner. The pressure perturbation is captured by employing a pressure-based semi-implicit algorithm for compressible flows [7].

*Corresponding author: kurose@mech.kyoto-u.ac.jp

Numerical Methods

Governing Equation

The governing equations for DNS with Arrhenius formulation solved for the gas phase are the conservation equations of mass, momentum, energy, and species mass written as [1],[2],[3],[4]

$$\frac{\partial \rho}{\partial t} + \nabla \cdot (\rho \boldsymbol{u}) = S_\rho, \tag{1}$$

$$\frac{\partial \rho \boldsymbol{u}}{\partial t} + \nabla \cdot (\rho \boldsymbol{u}\boldsymbol{u}) = -\nabla P + \nabla \cdot \boldsymbol{\sigma} + S_{\rho u}, \tag{2}$$

$$\frac{\partial \rho h}{\partial t} + \nabla \cdot (\rho h \boldsymbol{u}) = \frac{\partial P}{\partial t} + \boldsymbol{u} \cdot \nabla P + \nabla \cdot (\rho a \nabla h) + S_{\rho h}, \tag{3}$$

$$\frac{\partial \rho Y_k}{\partial t} + \nabla \cdot (\rho Y_k \boldsymbol{u}) = \nabla \cdot (\rho D_k \nabla Y_k) + S_{comb,k} + S_{\rho Y_k}, \tag{4}$$

and the equation of state. Here ρ is the density, $\boldsymbol{u}$ the gas-phase velocity, P the pressure, h the specific total enthalpy, a the gaseous thermal diffusivity, and Y_k and D_k the mass fraction and the mass diffusion coefficient of the k-th species, respectively. S_ρ, $S_{\rho u}$, $S_{\rho h}$ and $S_{\rho Y_k}$ represent the interactions between the gas and dispersed-droplets phases, and $S_{comb,k}$ is the source term due to combustion reaction, described later. The pressure, P, is calculated from the equation of state for an ideal gas. $\boldsymbol{\sigma}$ is the viscous stress tensor.

Individual fuel droplets are tracked in a Lagrangian framework. Concerning the vaporization of droplets, a hybrid model of a non-equilibrium Langmuir-Knudsen evaporation model [8],[9],[10] and a boiling evaporation model [11] is used. The governing equations for the droplet position, $\boldsymbol{x}_d$, velocity, $\boldsymbol{x}_d$, temperature, T_d, and mass, m_d, are given by

$$\frac{d\boldsymbol{x}_d}{dt} = \boldsymbol{u}_d, \tag{5}$$

$$\frac{d\boldsymbol{u}_d}{dt} = \frac{f_1}{\tau_d}(\boldsymbol{u} - \boldsymbol{u}_d), \tag{6}$$

$$\frac{dT_d}{dt} = \frac{Nu}{3Pr}\left(\frac{c_p}{c_{p,d}}\right)\left(\frac{f_2}{\tau_d}\right)(T - T_d) + \frac{1}{m_d}\left(\frac{dm_d}{dt}\right)\frac{L_V}{c_{p,d}}, \tag{7}$$

$$\frac{dm_d}{dt} = \begin{cases} -\dfrac{Sh}{3Sc}\dfrac{m_d}{\tau_d}\ln(1 + B_M) & T_d < T_B \\ -2\pi\dfrac{\lambda}{c_p}d_d(1 + 0.23Re_{sl}^{\frac{1}{2}})\ln\left\{1 + \dfrac{c_p(T - T_d)}{L_V}\right\} & T_d = T_B \end{cases}. \tag{8}$$

Here T is the gas temperature, T_B the boiling temperature of droplets, c_p the specific heat of mixture gas, $c_{p,d}$ the specific heat of the liquid, L_V the latent heat of vaporization at T_d. The particle response time, τ_d, is defined by

$$\tau_d = \frac{\rho_d d_d^2}{18\mu}, \tag{9}$$

where d_d is the droplet diameter. The Prandtl and Schmidt numbers in the gas phase are given by

$$Pr = \frac{\mu}{\rho a}, \qquad Sc = \frac{\mu}{\rho D_k}, \tag{10}$$

respectively. The Nusselt and Sherwood numbers are given by

$$Nu = 2 + 0.552Re_{sl}^{1/2}Pr^{1/3},$$

$$Sh = 2 + 0.552Re_{sl}^{1/2}Sc^{1/3}, \tag{11}$$

respectively. The droplet Reynolds number based on the slip velocity, $U_{sl} = |\boldsymbol{u} - \boldsymbol{u}_d|$, is defined as

$$Re_{sl} = \frac{\rho U_{sl} d_d}{\mu}. \tag{12}$$

The mass transfer number, B_M, is given by

$$B_M = \frac{Y_{V,S} - Y_V}{1 - Y_{V,S}}. \tag{13}$$

Here Y_V is the mass fraction of vapor on the far-field condition for droplets which is represented by the value in the cell where the droplet is located (this condition is the same for $\boldsymbol{u}$ and T), and $Y_{V,S}$ is the vapor surface mass fraction. The corrections of the Stokes drag and heat transfer for an evaporating droplet, f_1 and f_2, are given as [1],[12].

The phase coupling is implemented using a Eulerian-Lagrangian method. The phase coupling terms between the gas and dispersed-droplets phases, S_ρ, $S_{\rho u}$, $S_{\rho h}$, and $S_{\rho Y_k}$, are shown as

$$S_\rho = -\frac{1}{\Delta V}\sum_N \frac{dm_d}{dt}, \tag{14}$$

$$S_{\rho u} = -\frac{1}{\Delta V}\sum_N \frac{dm_d \boldsymbol{u}_d}{dt}, \tag{15}$$

$$S_{\rho h} = -\frac{1}{\Delta V}\sum_N \frac{dm_d h_d}{dt}, \tag{16}$$

$$S_{\rho Y_k} = -\frac{1}{\Delta V}\sum_N \frac{dm_d}{dt} \quad \text{for} \quad Y_k = Y_V, \tag{17}$$

where ΔV is the volume of the control volume for the gas-phase calculation, m_d the droplet mass, $\boldsymbol{u}_d$ the droplet velocity, h_d the specific total enthalpy of droplet, and N the number of droplets.

In this study, n-decane ($\mathrm{C_{10}H_{22}}$) is used as liquid spray fuel. The combustion reaction of the evaporated n-decane with oxygen is described using a one-step global reaction model [13] as

$$\mathrm{C_{10}H_{22}} + \frac{31}{2}\mathrm{O_2} \longrightarrow 10\mathrm{CO_2} + 11\mathrm{H_2O}, \tag{18}$$

and the reaction rate is given by the Arrhenius formulation as

$$\frac{\dot{m}_F}{W_F} = AT^n \exp\left(\frac{-E}{RT}\right)\left(\frac{\rho Y_F}{W_F}\right)^a \left(\frac{\rho Y_O}{W_O}\right)^b. \tag{19}$$

Here, $\dot{m}_F$ is the combustion rate of the fuel, W_F and W_O are the molecular weights of the fuel and oxidizer, respectively. A is the frequency factor, T the gas-phase temperature, and E the activation energy, and a, b, n the parameters depending on the fuel. In equation (4), the source term of the k-th species, $S_{comb,k}$, is expressed by the fuel consumption rate, $\dot{m}_F$, as

$$S_{comb,k} = -\frac{n_k}{n_F}\frac{W_k}{W_F}\dot{m}_F, \tag{20}$$

where n_k and n_F are the molar stoichiometric coefficients of the k-th species and the fuel in the one-step global reaction (positive for the productions), respectively. W_k and W_F are the molecular weights of the k-th species and fuel, respectively.

In order to take into account the effect of high internal pressure, boiling temperature, T_{BL}, and latent heat of vaporization, L_V, of liquid droplet at internal pressure of P are given by

$$T_{BL} = \left(\frac{P^{0.119} + c}{11.9}\right)^{-0.119}, \quad c = P_{atm} - 11.9T_{BL,atm}^{0.119}, \tag{21}$$

$$L_V = L_{V,T_{BL,atm}}\left(\frac{T_{CL} - T_d}{T_{CL} - T_{BL,atm}}\right)^{0.38}, \tag{22}$$

respectively. Here, the subscript atm means the value under atmospheric pressure. $L_{V,T_{BL}}$, T_{BL} and T_{CL} are the latent heat of vaporization, the boiling temperature and the critical temperature, respectively [1]. T_d is the droplet temperature. All thermo physical properties' values and transport coefficients under various pressures are obtained from CHEMKIN [14],[15].

Computational Details

Fig. 1 shows the schematic of computational domain and conditions. The computational domain is simplified model of a combustor, and the dimensions of the combustor are 76 mm and 14 mm in the x and y directions, respectively. A flame holder with 5 mm width is set at inlet of the combustor. The number of grid points set in combustor are 500 and 140 in the x and y directions, respectively. The grid size in the combustor for x and y directions are 150 μm and 100 μm, respectively. Air is injected from an inlet boundary. The temperature of air is 400 K, and the velocity at flame holder tip is 20 m/s. The Reynolds number based on the width of the flame holder and the inlet velocity is 6500. Fuel droplets are injected from tips of flame holder for x direction. The initial temperature is 300 K, and the velocity is 10 m/s. The equivalent ratio is set at 0.67. Each droplet's inlet diameter is given in a random manner from 1 μm to 16 μm.

In this study, inlet disturbance is given for velocity of air and fuel droplets, and mass flow rate of fuel droplets. Following equation is used for decide each value.

$$a = a_0(1 + A\sin(2\pi f t)). \tag{23}$$

Here, a stands for inlet air velocity, inlet fuel droplets' velocity and inlet fuel droplets' mass flow rate. a_0 is averaged value of each variable, A is the amplitude and f is the frequency of the disturbance. A ranges up to 0.5, and f is 800 Hz. In addition, non reacting cold flow cases are calculated as test calculations. Table1 lists the cases performed in this study. The magnitude of the disturbances ranges up to 50 % and the internal pressure is set at 0.1 or 0.5 MPa.

The governing equations of the carrier gas phase are discretized on a staggard mesh arrangement to construct fully conservative finite-difference formulations. The spatial derivatives in these equations are approximated by a second-order accurate central difference scheme. For the convection terms of the conservation equations of momentum, K.K. scheme is employed, and for the energy and mass fractions of chemical species, the QUICK scheme is employed. The fractional step method [7] and a third-order explicit Runge-Kutta method are used for the time advancement.

The CPU time for one case is about 70 h for 100,000 steps on Intel: Xeon L5640.

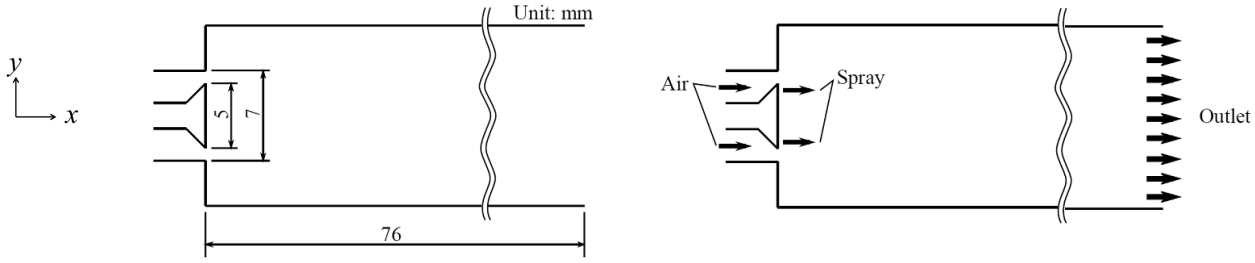

(a) Domain (b) Conditions

Figure 1. Computational domain and conditions.

Table 1. Cases performed in this study

Case	Combustion	Internal pressure [MPa]	Inlet velocity disturbance [%]
1	Cold flow	0.1	0
2	Cold flow	0.1	25
3	Cold flow	0.1	50
4	With combustion	0.1	0
5	With combustion	0.1	25
6	With combustion	0.1	50
7	With combustion	0.5	0
8	With combustion	0.5	25
9	With combustion	0.5	50

Results and Discussion

Cold flow cases

Fig. 2 shows the distributions of instantaneous streamwise gas velocity for cases 1-3. It is found that recirculation region is formed behind a flame holder. Fig. 3 shows the power spectra of pressure perturbation for cases 1-3. The peak of power spectra of pressure perturbation is observed to be located at 800 Hz for cases 2-3, and this frequency corresponds to the frequency of the inlet disturbance. Also, the peak for case 3 is more apparent than that for case 2. This means that this simulation code can correctly detect the pressure perturbation caused by the inlet velocity disturbance.

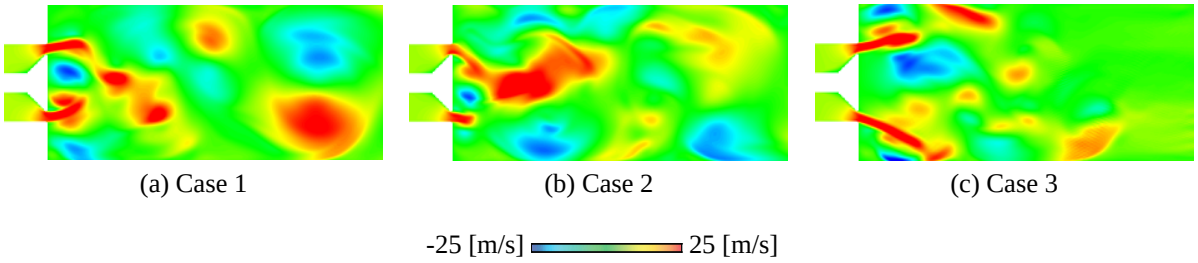

(a) Case 1 (b) Case 2 (c) Case 3

Figure 2. Distributions of instantaneous streamwise gas velocity for cases 1-3.

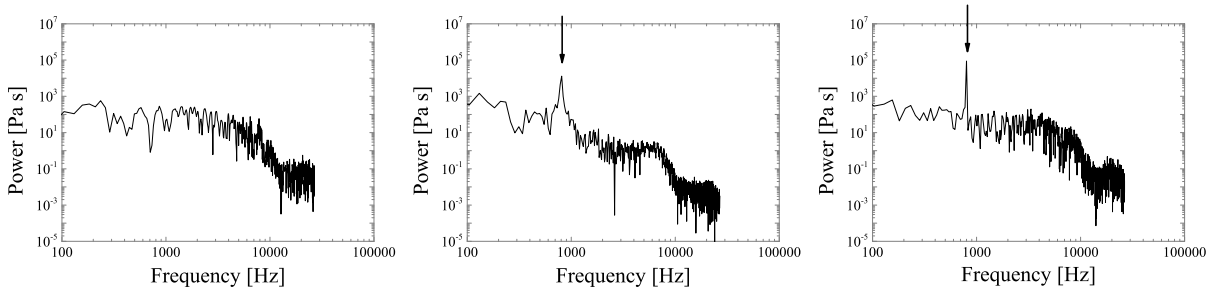

(a) Case 1 (b) Case 2 (b) Case 3

Figure 3. Power spectra of pressure for cases 1-3.

Effect of inlet disturbance

Fig. 4 shows the general features of spray flame, namely the distributions of instantaneous gas temperature, reaction rate and droplets for case 1. It is found that droplets evaporate upstream region and flame is formed behind the flame holder and on the corners of the combustor. High reaction rate is observed on the edges of flame.

The comparisons of instantaneous and time-averaged gas temperature for cases 4-6 are shown in Figs. 5 and 6. The gas temperature near the inlet tends to be increased by the disturbances of inlet flow and spray velocities. This reason is considered to be that mixing of air and fuel is promoted by the inlet disturbance and therefore the combustion reaction becomes more active.

Fig. 7 shows the power spectra of pressure perturbation for cases 4-6. The sampling point is located at the center of the combustor. For all cases, the peaks of power spectra of pressure perturbation are observed around 1200 Hz, and this frequency does not correspond to the frequency of the inlet disturbance of 800 Hz. The reason of the disagreement is considered due to that the pressure perturbation caused by combustion is much larger than that caused by the inlet disturbance. In fact, this frequency of 1200 Hz roughly agrees with the frequency of 1/4 mode of combustor length. This fact also means that the inlet disturbance, which is given independently of the pressure perturbation excited by combustion, do not affect the combustion behavior very much.

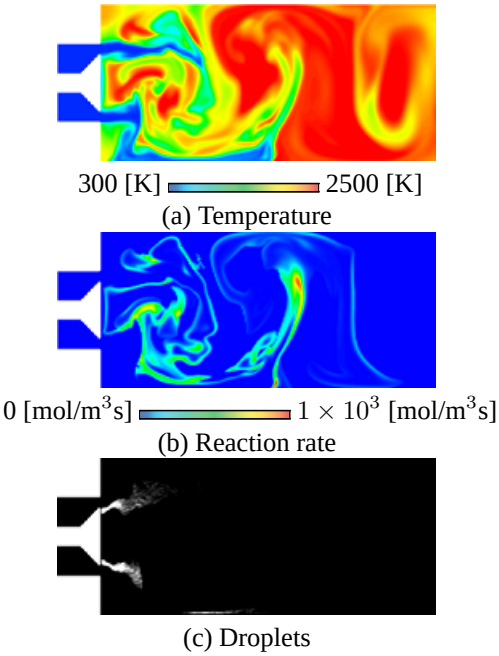

Figure 4. Distributions of instantaneous gas temperature, reaction rate and droplets for case 1.

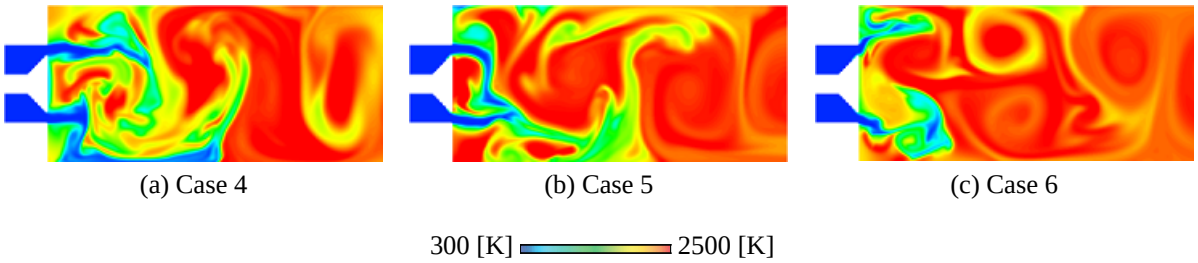

Figure 5. Distributions of instantaneous gas temperature for cases 4-6.

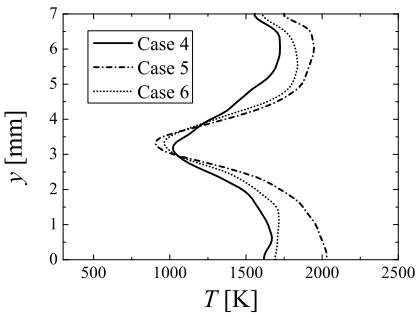

Figure 6. Distributions of time-averaged gas temperature at x=2 mm for cases 4-6.

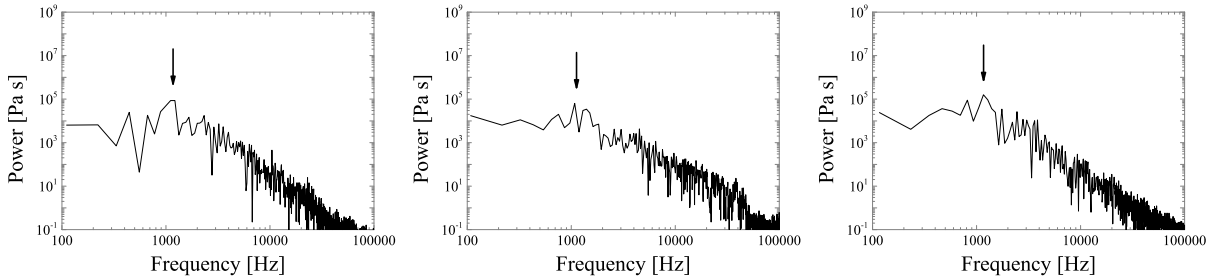

Figure 7. Power spectra of pressure for cases 4-6.

Effect of internal pressure

Figs. 8 and 9 show the distributions of instantaneous and time-averaged gas temperature for cases 7-9 for 0.5 MPa. Compared to cases 4-6 for 0.1 MPa (see Figs. 5 and 6), mixing is promoted and gas temperature near the inlet is higher. Also, the effect of the disturbances of inlet flow and spray velocities on the gas temperature near the inlet is smaller for cases 7-9 than that for cases 4-6. This is because the turbulence intensity and reaction rate increase with increasing the internal pressure and the effect is larger than that by the inlet disturbance.

The power spectra of pressure perturbation for cases 7-9 are shown in Fig. 10. Similarly to cases 4-6 for 0.1 MPa (see Fig. 7), the effects of the disturbances of inlet flow and spray velocities on the magnitude and frequency of the peak of power spectra of pressure perturbation for 0.5 MPa are not evident and the peaks appear around 1200 Hz for all cases. Due to the increase in the internal pressure, on the other hand, the magnitudes of the peaks are more remarkable and the pressure fluctuations are much higher because of the higher reaction rate.

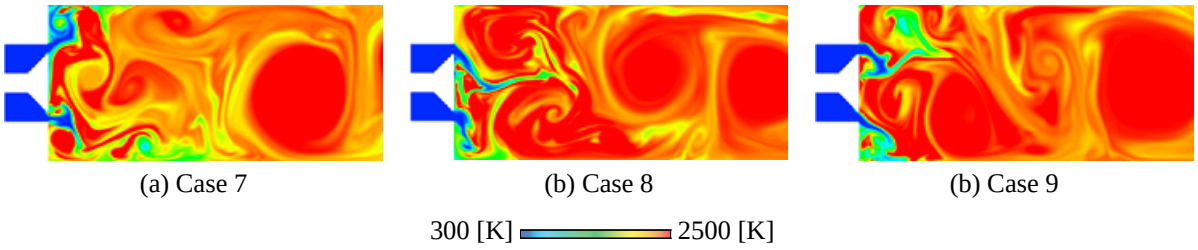

Figure 8. Distributions of instantaneous gas temperature for cases 7-9.

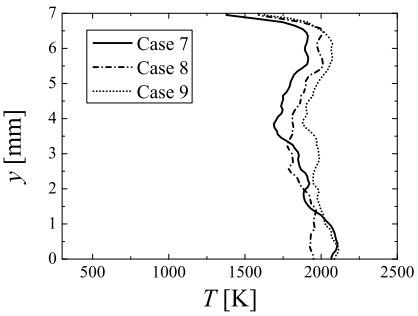

Figure 9. Distributions of time-averaged gas temperature at x=2 mm for cases 7-9.

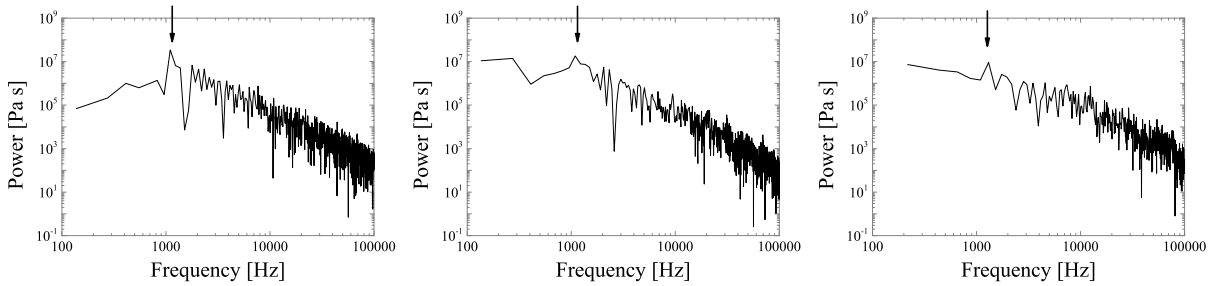

(a) Case 7 (b) Case 8 (b) Case 9

Figure 10. Power spectra of pressure for cases 7-9.

Summary and Conclusions

In this study, effects of disturbances of inlet flow and spray velocities and internal pressure on spray combustion field were investigated by means of two-dimensional direct simulation (DNS). The frequency and magnitude of the inlet disturbance were set at 800 Hz and up to 50 %, respectively, and the internal pressure was set at 0.1 or 0.5 MPa. The main results obtained in this study are summarized as follows.

1. The pressure perturbation in the spray combustion filed is enhanced by combustion reaction and increase in internal pressure, but it is not affected by disturbances of inlet flow and spray velocities very much.

2. The frequency indicating the peak of power spectra of pressure perturbation depends on neither the inlet disturbance nor the internal pressure.

Acknowledgements

A portion of this research was supported by "Strategic Programs for Innovative Research (SPIRE) - Research Field No. 4: Industrial Innovations" from the MEXT (Ministry of Education, Culture, Sports, Science, and Technology).

References

[1] Nakamura, M., Akamatsu, F., Kurose, R., Katsuki, M., *Physics of Fluids* 17:123301 (2005).
[2] Watanabe, H., Kurose, R., Hwang, S., Akamatsu, F., *Combustion and Flame* 148:234-248 (2007).
[3] Watanabe, H., Kurose, R., Komori, S., Pitsch, H., *Combustion and Flame* 152:2-13 (2008).
[4] Baba, Y., Kurose, R., *Journal of Fluid Mechanics* 612:45-79 (2008).
[5] Lieuwen,T.C., Yang, V., *Progress in Astronautics and Aeronautics* 210 (2005).
[6] de la Cruz García, M., Mastorakos, E., Dowling, A.P., *Combustion and Flame* 156:374-384 (2009).
[7] Moureau, V., Berat, C., Pitsch, H., *Journal of Computational Physics* 226:1256-1270 (2007).
[8] Bellan, J., Harstad, K., *International Journal of Heat and Mass Transfer* 30:125-136 (1987).
[9] Miller, R.S., Harstad, K., Bellan, J., *International Journal of Multiphase Flow* 24:1025-1055 (1998).
[10] Miller, R.S., Bellan, *Journal of Fluid Mechanics* 384:293-228 (1999).
[11] Kuo, K.K.Y., *Principles of Combustion* John Wiley and Sons, New York (1986).
[12] Kurose, R., Makino, H., Komori, S., Nakamura, M., Akamatsu, F., Katsuki, M., *Physics of Fluids* 15:2238-2351 (2003).
[13] Westbrook, C.K., Dryer, F.L., *Progress in Energy and Combustion Science* 10:1-57 (1984).
[14] Kee, R.J., Dixon-Lewis, G, Warnaz, J., Coltrin, M. E., Miller, J.A. *Sandia Report* SAND86-8246 (1986).
[15] Kee, R.J., Rupley, F.M., Miller, J.A., *Sandia Report* SAND89-8009B (1989).